ENSEMBLE FORECASTS AND VERIFICATION OF THE MAY 2015 MULTI-HAZARD SEVERE WEATHER EVENT IN OKLAHOMA

Austin Coleman[1], Nusrat Yussouf[2]

[1] National Weather Center Research Experience for Undergraduates Program, Norman, Oklahoma

[2] Cooperative Institute for Meteorological Studies, University of Oklahoma, and NOAA/OAR National Severe Storms Laboratory, Norman, Oklahoma

ABSTRACT

Dual threat severe weather events in which both tornadoes and flash floods affect the same area within a short time frame pose a complex problem since the life-saving actions for these two events are contradictory. One such event is the 6-7 May 2015 tornado and flash flood event over Oklahoma. This study explores the capability of a rapidly-updating 3-km horizontal grid spacing convective-scale ensemble data assimilation and prediction system developed as part of the Warn-on-Forecast initiative to forecast features of this dual threat severe weather event. Results indicate that the 0-1 h probabilistic forecasts of reflectivity verify reasonably well with the observations. However, beyond the 1 hour forecast period, the forecast accuracy is degraded, including biases in storm motion as well as spurious cell generation. The ensemble probability matched mean quantitative precipitation forecasts capture the placement of most intense areas of precipitation very well, but underestimate the amount of accumulated precipitation. These quantitative precipitation forecasts are found to outperform the deterministic quantitative precipitations forecasts of the operational High-Resolution Rapid Refresh model as well. Additional ensemble forecast experiments from simple downscaling to 1-km grid spacing from the 3-km ensemble do not significantly reduce the storm motion bias found in the original results and introduce more spurious cells.

1. INTRODUCTION

The Warn-on-Forecast (WoF) is a NOAA funded project which seeks to provide National Weather Service (NWS) forecasters with numerical model guidance that will enable longer lead times, greater accuracy, and probabilistic rather than deterministic forecasts and warnings of severe convective hazards. One of the goals of WoF is to develop a rapidly updating, convective-scale ensemble data assimilation and prediction system. Much of the early work since the beginning of the WoF project in 2009 was focused on 0-1 h forecasts of storm tracks and low-level mesocyclones of tornadic convective events (Dawson et al. 2012; Yussouf et al. 2013, 2015; Skinner et al. 2016). While tornadoes can be the most violent convective hazard and one of the most challenging phenomena to predict, the technology and science being developed to achieve the WoF goal will likely improve the prediction of other convective weather hazards as well.

One such weather hazard is flash flood producing extreme rainfall from convectively driven events. Floods and

[1] *Corresponding author address:* Austin Coleman, Meteorology Department, Valparaiso University, 1509 Chapel Drive, Valparaiso, IN 46383
Email: austin.coleman@valpo.edu

especially flash floods typically result in more deaths each year than from tornadoes, hurricanes, lightning, or straight line winds. Severe weather hazards are particularly dangerous when there are multiple threats, with tornadic and flash flood combination events likely being the deadliest.

The tornado and flash flood event from 6-7 May 2015 in central Oklahoma is one such event. The goal of this study is to evaluate the capability of a prototype WoF system in forecasting both of these hazards. Furthermore, the ultimate goal of WoF is to predict tornadic circulations, which is expected to require sub 100 m horizontal grid spacing (Bryan et al. 2003). The current prototype WoF system uses a 3-km horizontal grid spacing due to computational constraints. Another goal of this study is to evaluate how the forecasts perform at a higher resolution with 1-km grid spacing. A preliminary grid spacing sensitivity examination is conducted to determine whether nesting down from 3-km to 1-km grid spacing without additional data assimilation significantly changes the forecasts.

An overview of the 6-7 May 2015 Oklahoma tornado and flash flood event is summarized in Section 2 followed by the methodology used to conduct the study in Section 3. Results are examined and discussed in Section 4 and conclusions with broader implications of the results and future work is found in Section 5.

2. 6-7 MAY 2015 OKLAHOMA TORNADO AND FLASH FLOOD EVENT

There was widespread severe weather activity during 6-7 May 2015 over the central plains, with central Oklahoma being impacted by multiple threats (Fig. 1a). Sixteen tornadoes were confirmed by the Norman NWS in an area extending from northern Texas into northern Oklahoma. Of these sixteen, eleven were rated EF0, two were rated EF1, one was rated EF2, and two were rated EF3s. Of these tornadoes, the Bridge Creek/Amber EF3 (referenced hereafter as the Bridge Creek tornado) is the tornadic focal point of this study. It began at 2133 UTC, or 0433 PM CDT and tore a 10 mile path through northern Grady county, with dissipation occurring around 2226 UTC (0526 PM). The other EF3 touched down a few hours later at 0141 UTC (0841 PM) in southeast Oklahoma City. This tornado was brief with only a 2-mile path length and a 7-minute lifetime.

This event was particularly unique in that supercells were slow-moving and back building in nature (Fig. 1b-c). The main initial supercell continuously initiated new updrafts on its western flank throughout the afternoon and into the evening hours. The continuous back building of supercells is curious in itself, given that typically one strong supercell will stabilize the atmosphere enough to prevent further convective initiation in the hours immediately following.

The tendency for this large supercellular storm cluster to continuously back build and thus remain quasi-stationary, combined with the environment's ample moisture availability led to heavy rainfall rates over the same few counties for extended periods of time. Consequently, major flash flooding occurred in a handful of counties, with several flash flood reports occurring between 2356 and 0230 UTC. To make matters worse, the flash flooding occurred very closely

to the areas in which many of the tornadoes occurred throughout the evening. These two threats pose a complicated problem for forecasters in that the threats require two contradictory lifesaving actions. A tornado warning warrants that people seek underground shelter whereas a flash flood warning warrants that people seek higher ground. It is imperative that events like these are forecast with precision and accuracy so that people affected will always have the correct plan of action to take.

(a)

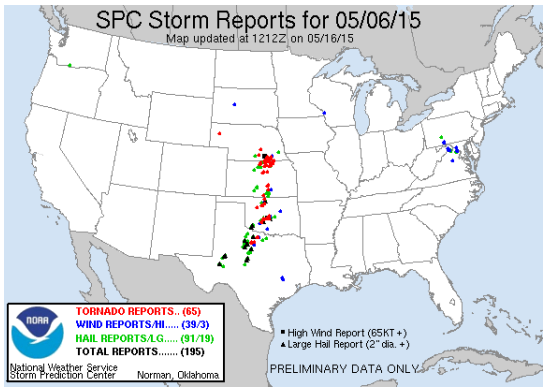

(b)

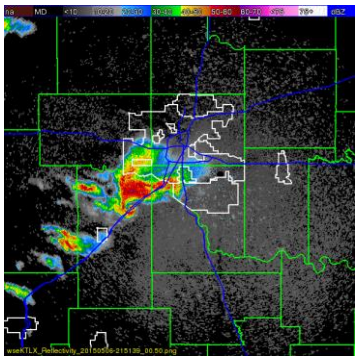

(c)

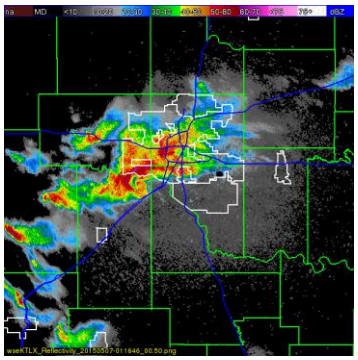

FIG. 1. (a) SPC Storm Reports for May 6, 2015 over the continental United States. (b) Twin Lakes, Oklahoma reflectivity image valid at 2151 UTC (0451 PM CDT) with well-defined hook echo in northeast Grady county. (c) Reflectivity image valid at 0116 UTC (0916 PM CDT) depicting another well-defined hook echo in northeast Grady county as well as indications of other mesocyclones in the vicinity of the main hook. The cyclic, back-building nature of this series of supercells persisted for a matter of hours before finally growing up-scale and propagating eastward out of central Oklahoma.

3. METHODOLOGY

This case study utilizes a prototype WoF system based on the Advanced Research Weather Research and Forecasting model, specifically WRF-ARW version 3.6.1 (Skamarock 2008). A 3-km storm-scale domain is one-way nested within a 15-km mesoscale domain. There are 50 vertical levels in both domains that extend to 100 hPa. The ensemble is initialized at 0000 UTC on 6 May 2015 from the National Center for Environmental Prediction's (NCEP) Global Ensemble Forecast System (GEFS) analyses. The first 18 of 20 members from the GEFS are doubled to create a multiphysics ensemble system with 36 members. In this way, the GEFS is used to provide the initial conditions for both the storm-scale and mesoscale domains simultaneously. After the

model is initiated, the mesoscale domain becomes the source of boundary conditions for the storm-scale domain. The physics parameterization schemes are the same for both domains, except for the cumulus parameterization schemes which are turned off for the 3-km storm-scale domain in order to allow convection. Further details on the physics schemes used in this study can be found in Yussouf et al. (2015) and Yussouf et al. (2016).

The ensemble adjustment Kalman filter (EAKF) is implemented with the Data Assimilation Research Testbed software system (Anderson 2001; Anderson and Collins 2007) to perform hourly data assimilation of conventional observations into both domains simultaneously (Yussouf et al. 2016).

Around the time of convective initiation (i.e. 1800 UTC), reflectivity and radial velocity observations from the operational WSR-88D radars are assimilated at 15 minute intervals into the storm-scale domain using EAKF. Very short-term ensemble forecasts are launched every 30 minutes after 90 minutes of radar data assimilation.

Probabilistic reflectivity forecasts are verified with Multi-Radar Multi-Sensor System (MRMS) observations (Zhang et al. 2011). Probabilistic vorticity forecasts are verified with a shapefile of the Bridgecreek tornado damage path obtained from the NWS damage survey. Ensemble probability matched mean (PMM) quantitative precipitation forecasts (QPFs) are compared with both NCEP Stage IV precipitation analysis and Oklahoma mesonet observations. QPFs are also compared with forecasts from the operational High-Resolution Rapid Refresh (HRRR) model.

In addition to ensemble forecasts at 3-km grid spacing, ensemble forecasts are also evaluated at 1-km grid spacing. The 1-km storm-scale ensemble is initialized by nesting down from the 3-km domain, which is used for the initial and boundary conditions. No data assimilation is conducted in the 1-km nested domain.

4. RESULTS

4.1 *Probabilistic Reflectivity Forecasts*

The ensemble forecast probabilities of reflectivity exceeding a threshold of 40 dBZ are evaluated and verified with radar observations at 3-km resolution for three initialization times: 2100 UTC (Figs. 2a-c), 2045 UTC (Figs. 2d-f) and 2030 UTC (Figs. 2g-i). The ensemble forecasts initialized at 2100 and 2045 UTC (Figs. 2a, d) maintain the core of the storm with relatively high probabilities (>75%) during the initial 30-45 minutes of the forecasts. Later in the forecast period probabilities start to decrease as ensemble members begin to diverge in their solutions (Figs. 2 b-c, e-i, and g-h). The highest probabilities of intense reflectivity are displaced to the east of the observed reflectivity contour, which is indicative of an eastward storm motion bias. This is a common error with storm-scale data assimilation and prediction systems (Yussouf et al. 2015, 2016). In addition, as new observed storm cores are generated off of the western flank of the main storm further into the forecast period, there is no sign of the ensemble generating these new storm cores (Figs. 2c, f, and i). This is not surprising seeing as NWP models have known difficulties forecasting convective initiation.

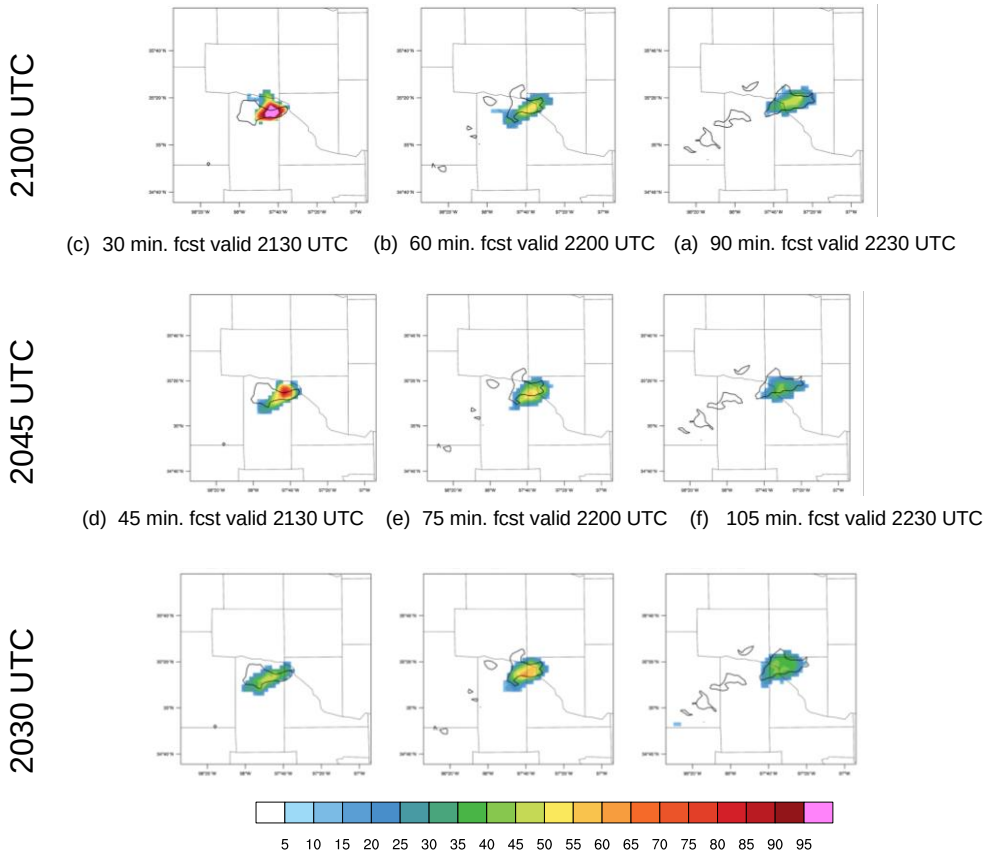

(c) 30 min. fcst valid 2130 UTC (b) 60 min. fcst valid 2200 UTC (a) 90 min. fcst valid 2230 UTC

(d) 45 min. fcst valid 2130 UTC (e) 75 min. fcst valid 2200 UTC (f) 105 min. fcst valid 2230 UTC

(g) 60 min. fcst valid 2130 UTC (h) 90 min. fcst valid 2200 UTC (i) 120 min. fcst valid 2230 UTC

FIG. 2. Forecast probabilities of reflectivity exceeding 40 dBZ at 1500 m above mean sea level (MSL; colors, 5% increment) from three different initialization times (black contour overlaid is the MRMS observed 40 dBZ reflectivity) extending to 2230 UTC. (a)-(c) are forecast output at 30 minute intervals from the 2100 UTC initialization time, (d)-(f) from the 2045 UTC initialization time, and (g)-(i) from the 2030 UTC initialization time.

4.2 *Probabilistic Vorticity Forecasts at 3 km Grid-Spacing*

The forecast probability of vorticity greater than 0.002 s^{-1} at 1500 m above ground level is used as a proxy for tornado potential for this study (Yussouf et al. 2015, 2016). Three different forecast initialization times are compared among the runs – 2100 (Fig. 3a), 2045 (Fig. 3b), and 2030 UTC (Fig. 3c), which represent 33-minute, 48-minute, and 63-minute lead times respectively for the Bridgecreek tornado. All probabilistic vorticity swaths extend from their respective initialization times to 2230 UTC, which is 4 minutes after the estimated dissipation of the Bridgecreek tornado.

The forecast initialized at 2100 UTC (Fig. 3a) shows the higher probabilities of vorticity exceeding the threshold well to the southwest of the actual tornado damage path. This was found to coincide with the analysis time (not shown), where virtually all members agreed on the placement of the mesocyclone. This speaks for the data assimilation system, showing that all members are analyzing the supercellular characteristics of the storm well. The beginning of the tornado

damage path is collocated with 40-45% probability. However, the magnitude of probabilities starts to decrease during the forecasts as member forecasts diverge with time, resulting in low certainty for the majority of the tornado's damage path.

With each earlier initialization time (Figs. 3b-c), it is found that the highest certainties coincide with the analysis time as well. As expected, certainties approaching the tornado damage path are less with longer lead times. There is also an additional high probability vorticity swath to the north of the main swath for 2030 and 2045 UTC initialization times (Figs. 3b-c), which does not verify with a reported tornado.

Nevertheless, each ensemble forecast does recognize and maintain the main mesocyclone associated with the Bridgecreek tornado. While certainty at the point of Bridgecreek tornadogenesis is not impressive for any of the lead times, the recognition of the mesocyclone well in advance of tornadogenesis and the northeastward propagation of the vorticity probabilities is still a very useful tool for forecasters to identify a potentially tornadic storm.

(a) 21:00 – 22:30 UTC (30 min. lead time)

(b) 20:45 – 22:30 UTC (45 min. lead time)

(c) 20:30 – 22:30 UTC (60 min. lead time)

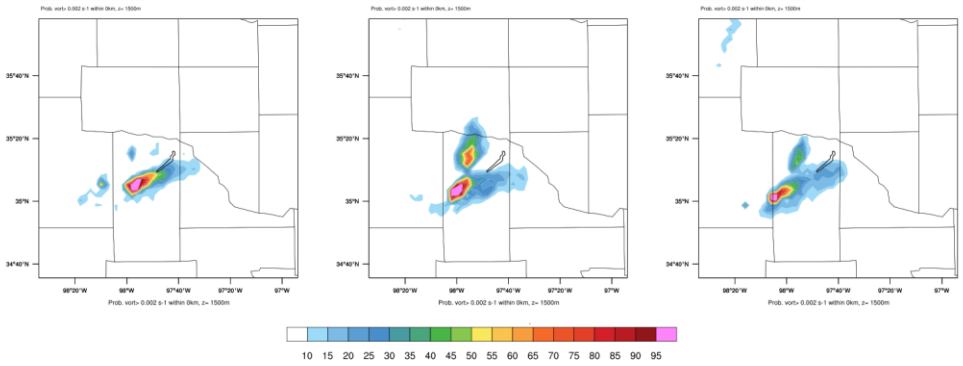

FIG. 3. Forecast probabilities (in percent) of vorticity exceeding 0.002 s^{-1} to 2230 UTC. Initialization times include 2100 (a), 2045 (b), and 2030 (c) UTC. The black contour overlaid represents the NWS Bridgecreek tornado damage path (2133 – 2226 UTC).

4.3 *1-h Quantitative Precipitation Forecasts*

To determine the ensemble's ability to predict the extreme precipitation associated with this flash flood event, QPFs are launched from different initialization times as described previously. To best represent all of the ensemble member QPFs in a deterministic way, the probability matched mean (PMM; Ebert 2001) of the QPFs is calculated.

Because the heaviest rainfall during that night occurred between 0000 and 0300 UTC, with particularly heavy rainfall occurring between 0200 and 0300 UTC, this 3-h time frame will be the focus of the QPF study. The 1-h PMM QPFs are compared with NCEP's Stage IV 1-h precipitation accumulation analyses. The sizes, shapes, and placements of the areas of forecast precipitation for all three forecasts (Figs. 4b, e, and h) are similar to those seen in the observations (Figs. 4a, d, and g). However, difference plots that show

areas of underestimation and overestimation of the forecast with respect to the observations suggest an underestimation bias for both the 0000-0100 UTC forecast (Fig. 4c) and the 0200-0300 UTC (Fig. 4i) forecast.

Curiously, the 1-h QPF valid from 0100-0200 UTC shows the smallest forecast error (Fig. 4f). Therefore, the skill of the ensemble forecasts may vary at different initialization times.

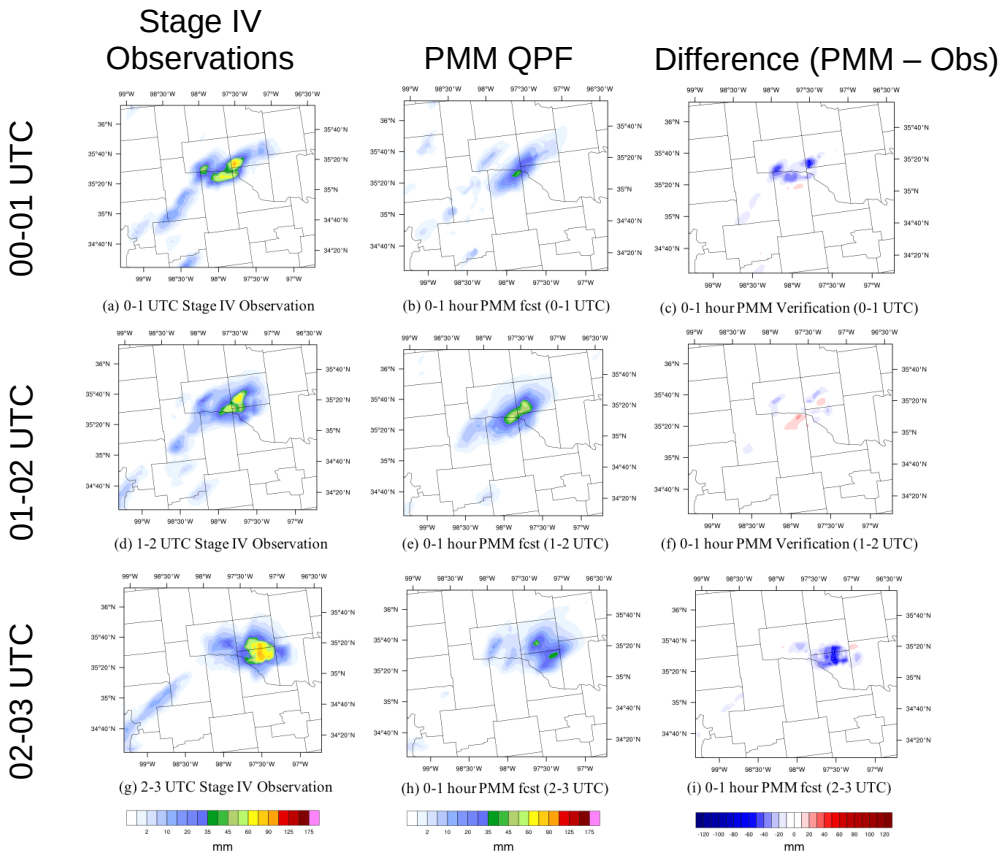

FIG. 4. Verification of 1-h QPFs using probability matched means (b), (e), (h) initialized at 00, 01, and 02 UTC. The NCEP's Stage IV analyses are shown in (a), (d), and (g). Difference plots are shown in (c), (f), and (i).

4.4 *Comparison with operational HRRR QPFs*

The 0-3 h rainfall forecast from the operational HRRR QPF (Fig. 5b) shows a northward displacement of highest forecast precipitation accumulations compared to the Stage IV analysis. The HRRR overforecasts to the north of the observations and underforecasts where the intense precipitation actually occurred (Fig. 5d). In contrast, the 0-3 h QPF from the PMM (Fig. 5c) is placed approximately correctly with respect to the observations, although the bullseye of most intense precipitation core is slightly displaced to the south as compared to the observations. However, the precipitation underestimation bias is still present (Fig. 5e) in this 3-h forecast, and a local maximum in observed precipitation over northeast Cleveland

county is not captured by the ensemble system.

In addition, the 3-h forecast time series of rainfall maxima for the Oklahoma City East mesonet station are calculated for both the HRRR and WoF systems utilizing a neighborhood approach with a 6 km radius. These are compared with the mesonet station rainfall observation (Fig. 6). The forecasts initialized at 0000 UTC (Fig. 6a) indicate that the mesonet observation remains on the edge of or outside of the ensemble envelope, indicating underestimation of the QPFs in the ensemble system. The ensemble mean of the maximum QPFs also depicts an underestimation bias that grows more pronounced with each hour of the forecast period. The maximum HRRR QPF heavily underestimates the accumulated precipitation. After the first hour of the forecast, the HRRR predicts lower precipitation accumulation values than any of the WoF ensemble members.

The ensemble mean time series of maximum QPFs initialized at 0200 UTC (Fig. 6b), actually slightly over estimates the total accumulated precipitation with respect to the observation in the first hour of the time series. The observation lies at the lower edge of the ensemble envelope QPF spectrum. After the first forecast hour, the underestimation bias from the ensemble appears again, but is less pronounced as observed rainfall accumulation begins to decrease for the last two hours of the time series. The HRRR QPF under predicts the accumulated precipitation values for the duration of the forecast.

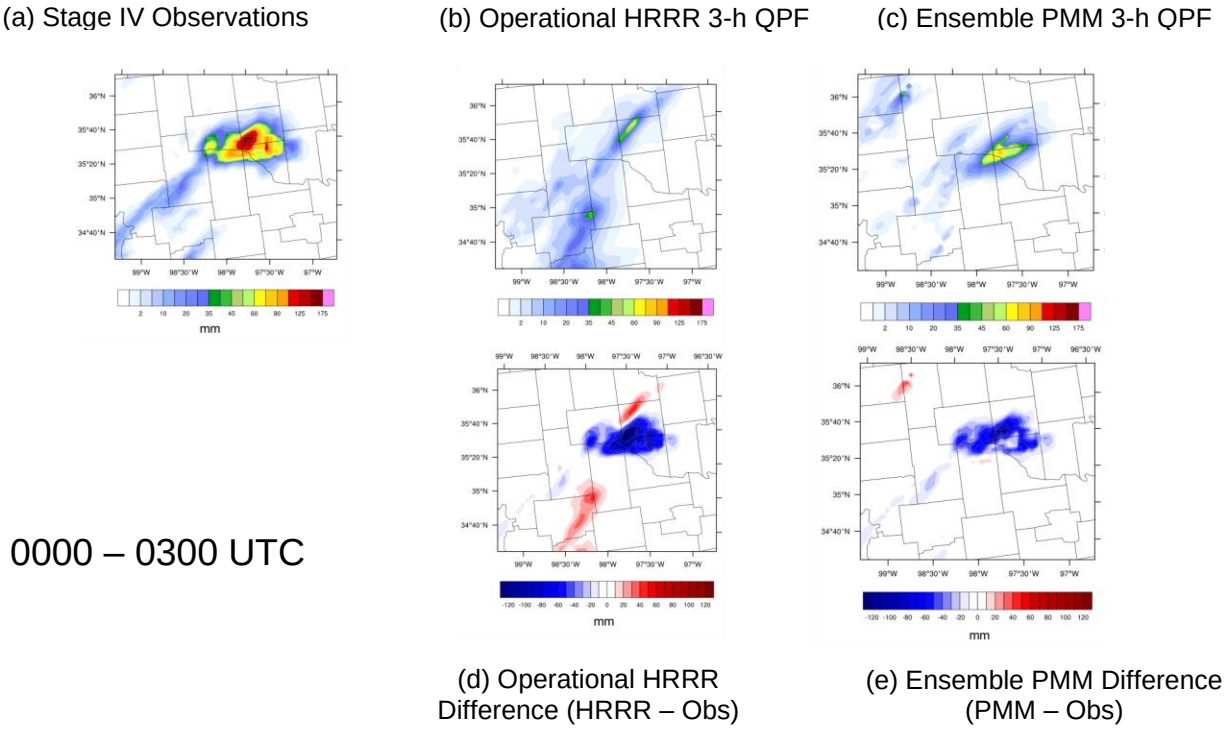

FIG. 5. 3-h Stage IV rainfall (a), operational 3-h HRRR QPF (b) with respective difference plot (d), and 3-h PMM QPF (c) with respective difference plot (e).

(a) 0000-0300 UTC Mesonet Timeseries with 6 km neighborhood

(b) 0200-0500 UTC Mesonet Timeseries with 6 km neighborhood

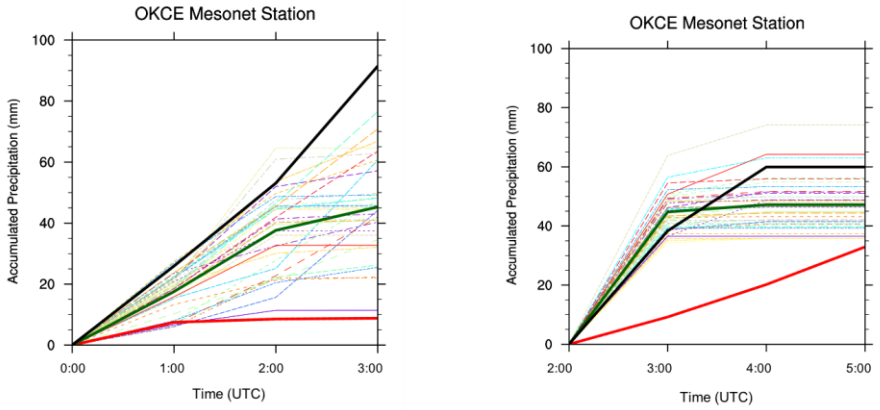

FIG. 6. QPFs from ensemble members using a 6 km neighborhood approach (thin multi-colored lines) against mesonet observations from the Oklahoma City East mesonet site (black line). The ensemble mean of maximum ensemble member QPFs (green line) and the maximum HRRR QPF using the same neighborhood approach (red line) is plotted.

4.5 *Reflectivity Forecasts from 3-km and 1-km Grid Spacing Ensembles*

To determine whether a higher resolution storm-scale model adds any value, 1-km horizontal grid-spacing ensemble forecasts are generated in a one-way nested setup within the 3-km storm-scale ensemble. After initializing the 1-km domain, the 3-km domain simply provides the boundary-conditions for the 1-km nest and no additional data assimilation is performed. We pose the question – can nesting down further to 1-km without additional data assimilation at 1-km grid spacing add any value? Results indicate that the forecasts from a typical ensemble member (member 33 is chosen randomly) generate even more spurious cells in southwest Oklahoma from the 1-km runs (Fig. 7c) than from the 3-km runs (Fig. 7b) when compared with the observations (Fig. 7a). Furthermore, the spurious cells produced in the 1 km domain are rotating as evidenced by the contours of vertical vorticity exceeding 0.004 s^{-1}. These additional spurious cells and spurious mesocyclones are identified in all ensemble member forecasts at 1-km grid spacing, implying that further studies on 1-km grid spacing ensembles are needed in the future.

4.6 *Probabilistic Vorticity Forecasts from 3-km and 1-km Grid Spacing*

A comparison of probabilistic vorticity swaths reveals that probabilities intersecting the Bridgecreek tornado damage path from the 1-km forecast (Fig. 8b) are not higher than those resulting from the 3-km forecast (Fig. 8a) for the 30-minute lead time. To identify how the forecasts differ when analyzing the mesocyclone at the time of tornadogenesis, probabilistic vorticity forecasts were initialized 3 minutes prior to tornadogenesis. Higher probability swaths are collocated with the tornado damage path in the 3-km forecast (Fig. 8c) compared to that from the 1-km forecast (Fig. 8d). However, neither forecasts capture the left turn in the tornado's path with high certainty.

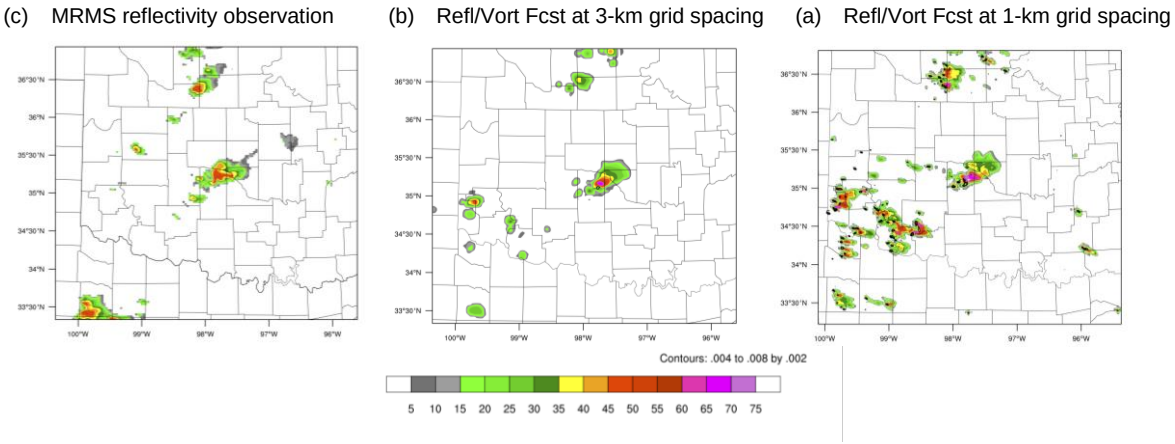

FIG. 7. The MRMS reflectivity observations (a) and reflectivity forecasts from 3-km (b) and 1-km (c) grid spacing at 3 km MSL for ensemble member 33. The black contours overlaid are vorticity incremented from 0.004 to 0.008 s^{-1} by 0.002 s^{-1}.

Furthermore, the 1-km forecast is very noisy as a result of spurious cells. High probabilities are found in both 1-km forecasts to the north of the main probabilistic vorticity swath.

5. DISCUSSION AND CONCLUSIONS

The ability of a prototype WoF system to predict storm intensity, supercellular features and extreme precipitation is evaluated. Probabilistic reflectivity forecasts show the ensemble's ability to maintain the intensity of the Bridgecreek supercell. However, an eastward displacement bias is seen as well as inadequacy in forecasting the training nature of the convective cells.

The QPFs from the prototype system outperform those from the operational HRRR for this case and forecast similar size, shape, and placement of precipitation with respect to the observations. However, a precipitation underestimation bias is seen and is likely systematic with this ensemble system. To discover what is causing this error, further studies must be conducted. Dahl and Xue (2016) isolate some biases concerning the Thompson microphysics scheme in a case study from 2010. In this study, it was found that ensemble members with Thompson showed less skill and lower precipitation forecasts than ensemble members with other microphysics schemes. However, this relative lack of skill was attributed to a late bias in which a mesoscale convective system propagated more slowly in the forecast than observed, whereas in our case we see a slight eastward displacement bias in which storms move slightly more quickly than observed. In the future, a microphysics sensitivity study will likely be needed for this system to diagnose and solve this underestimation bias. Grid-spacing sensitivities will also need to be explored to evaluate the optimal grid spacing required to forecast this type of event.

Despite the bias, successful placement of the most intense precipitation accumulations through 1-h and 3-h forecasts has good implications for the forecasting community. The ability to identify locations of intense precipitation accumulation in advance of an event could allow forecasters to increase flood lead times.

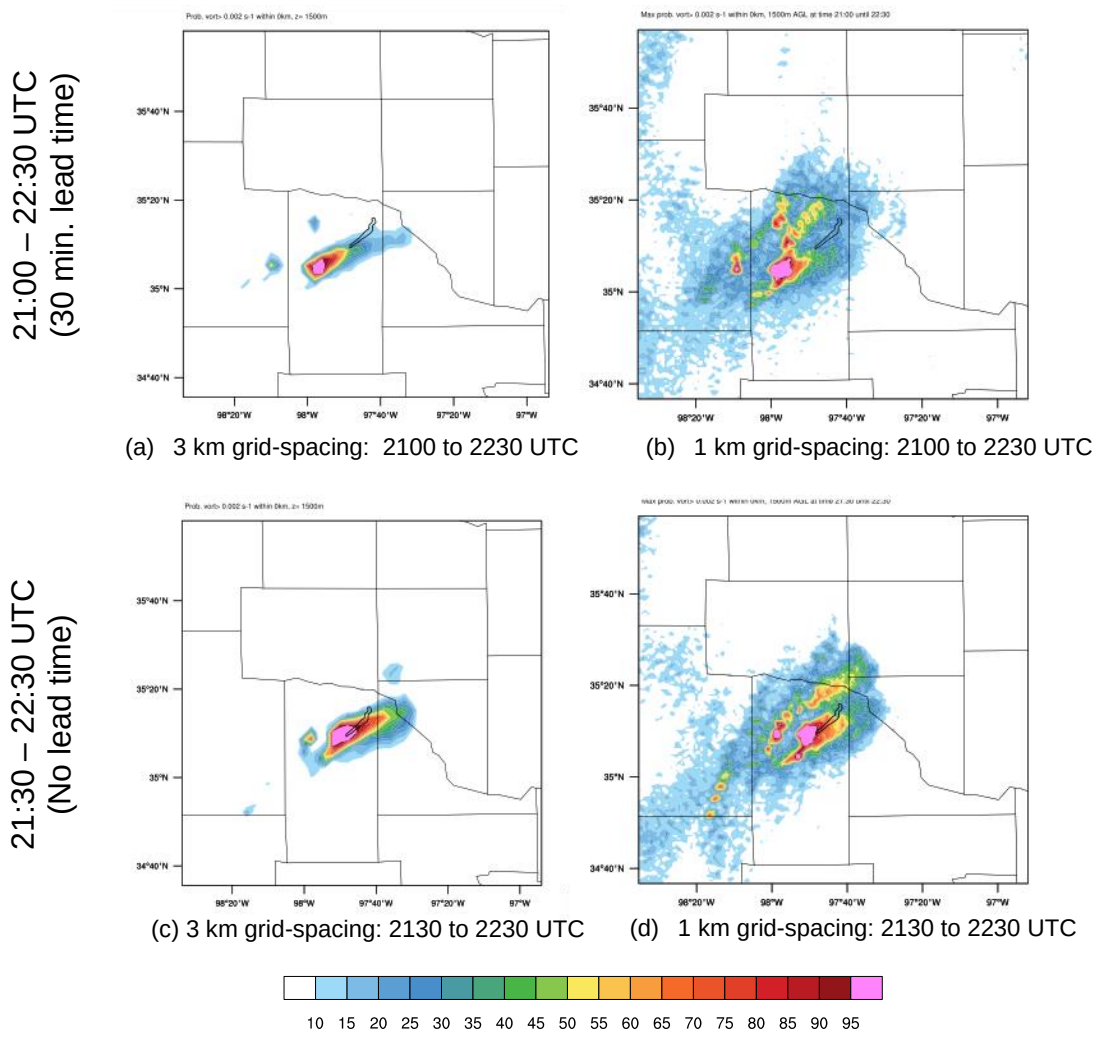

FIG. 8. Probabilistic vorticity swaths as in Fig. 3 but between the 3-km and 1-km runs.

There is also potential benefit in forcing hydrologic models with the WoF system for longer probabilistic forecast lead times of flash floods.

For forecasting low-level rotation associated with the Bridgecreek mesocyclone, forecasts from multiple initialization times and grid spacings are compared and verified against the Bridgecreek tornado damage path. While results are preliminary and further investigations into the most robust nesting techniques are needed for a thorough conclusion, it is also important to evaluate if radar data assimilation at 1-km grid spacing is needed.

The ultimate goal of the Warn-on-Forecast is to move toward an ensemble with <1-km grid spacing in an effort to resolve tornadic circulation that can be run in real-time operationally. This is done in the hopes of extending tornado and flash flood lead times in conjunction with NOAA's goal to save lives and property.

6. ACKNOWLEDGEMENTS

The author would like to thank Dr. Thomas Jones for answering many questions, Greg Blumburg for the presentation advice, and Cameron

Nixon for the helpful convective dynamics discussions.

This work was prepared by the authors with funding provided by National Science Foundation Grant No. AGS-1560419 and NOAA/Office of Oceanic and Atmospheric Research under NOAA-University of Oklahoma Cooperative Agreement #NA11OAR4320072, U.S. Department of Commerce. The statements, findings, conclusions and recommendations are those of the author(s) and do not necessarily reflect the views of the National Science Foundation, NOAA, or the U.S. Department of Commerce.

7. REFERENCES

Anderson, J. L., 2001: An ensemble adjustment Kalman filter for data assimilation. *Mon. Wea. Rev.*, **129,** 2884–2903.

Anderson, J. L., and N. Collins, 2007: Scalable implementations of ensemble filter algorithms for data assimilation. *J. Atmos. Oceanic Technol.*, **24**, 1452–1463.

Bryan, G. H., Wyngaard, J. C., and Fritsch, J. M.: Resolution Requirements for the Simulation of Deep Moist Convection. *Mon. Wea. Rev.,* **131,** 2394-2416. doi:10.1175/1520-0493(2003)131<2394:RRFTSO>2.0.CO;2

Dahl, N., Xue, M.: Prediction of the 14 June 2010 Oklahoma City Extreme Precipitation and Flooding Event in a Multi-Physics Multi-Initial Condition Storm Scale Ensemble Forecasting System. *Wea. Forecasting.*

Dawson, D. T., Wicker, L. J., Mansell, E. R.: Impact of the Environmental Low-Level Wind Profile on Ensemble Forecasts of the 4 May 2007 Greensburg, Kansas, Tornadic Storm and Associated Mesocyclone. *Mon. Wea. Rev.,* **140,** 696-716. doi:10.1175/MWR-D-11-00008.1.

Ebert, E.: Ability of a Poor Man's Ensemble to Predict the Probability and Distribution of Precipitation. *Mon. Wea. Rev.,* **129,** 2461-2480.

Skamarock, W. C., and Coauthors, 2008: A description of the Advanced Research WRF version 3. NCAR Tech. Note NCAR/TN-475+STR, 133 pp.

Skinner, P. S., Wicker, L. J., Wheatley, D. M., and Knopfmeier, K. H.: Application of Two Spatial Verification Methods to Ensemble Forecasts of Low-Level Rotation. *Wea. Forecasting,* **31,** 713-735.

Stensrud, D. J., and Coauthors, 2012: Progress and challenges with Warn-on-Forecast. Accessed 28 July 2016. [Available online at http://twister.ou.edu/papers/Stensrud_etal_AR2013.pdf.]

Yussouf, N., Dowell, D., and Wicker, L., 2015: Storm-Scale Data Assimilation and Ensemble Forecasts for the 27 April 2011 Severe Weather Outbreak in Alabama. *Mon. Wea. Rev.,* **143,** 3044-3066.

Yussouf, N., Kain, J., Clark, A., 2016: Short-term Probabilistic Forecasts of the 31 May 2013 Oklahoma Tornado and Flash Flood Event Using a

Continuous-Update-Cycle Storm-scale Ensemble System.

Yussouf, N., Mansell, E. R., Wicker, L. J., Wheatley, D. M., Stensrud, D. J.: The Ensemble Kalman Filter Analyses and Forecasts of the 8 May 2003 Oklahoma City Tornadic Supercell Storm Using Single- and Double-Moment Microphysics Schemes. *Mon. Wea. Rev.,* **141,** 3388-3412.

Zhang, J., and Coauthors, 2011: National Mosaic and Multi-Sensor QPE (NMQ) system: Description, results, and future plans. *Bull. Amer. Meteor. Soc.,* **92,** 1321–1338, doi:10.1175/2011BAMS-D-11-00047.1.